Earth and Planetary Science Letters 450 (2016) 40–51

Contents lists available at ScienceDirect

Earth and Planetary Science Letters

www.elsevier.com/locate/epsl

Abnormal seismological and magmatic processes controlled by the tearing South American flat slabs

Jiashun Hu *, Lijun Liu

Department of Geology, University of Illinois at Urbana–Champaign, 605 E. Springfield Ave, Champaign, IL, 61820, USA

ARTICLE INFO

Article history:
Received 31 December 2015
Received in revised form 13 June 2016
Accepted 14 June 2016
Available online xxxx
Editor: P. Shearer

Keywords:
aseismic ridge
slab tear
adakite
seismic tomography
Peruvian flat slab
Central Chile flat slab

ABSTRACT

The influence of flat slab subduction on the formation of intra-slab earthquakes, volcanic activities and mantle seismic velocity anomalies remains unclear. We attempt to better understand these processes by simulating the two flat slabs in Peru and Chile using data-orientated geodynamic models. Our results successfully reproduce the observed flat slabs as mainly due to two subducting aseismic ridges. In contrast to the traditional view of flat-slab subduction, we find that these slabs are internally torn, as is due to the 3D nature of the subducting buoyancy features. This broken slab configuration, confirmed by regional tomography, naturally explains the abnormal distribution of and stress regimes associated with the intermediate-depth earthquakes. We further show that the slab tearing process could also better explain the formation of adakitic and ore-forming magmatism, the evolution of the magmatic arc, and the enigmatic mantle seismic structures beneath these regions. We propose that slab tearing may represent a common result of buoyancy feature subduction and that the resulting mantle processes could affect the long-term geodynamic evolution of continents.

1. Introduction

The formation of flat slabs strongly affects the volcanic history, earthquake generation, and ore deposits along convergent plate boundaries. In South America, the two most prominent flat slabs, located in Peruvian and Central Chilean (Fig. 1), display several unique characteristics, which apparently deviate from the traditional understanding of flat-slab subduction. First, the distribution of intra-slab seismicity and volcanic activities (Fig. 1a) along the South American subduction zone, especially at these two flat-slab segments, show irregular spatial patterns (Brudzinski and Chen, 2005; Gutscher et al., 1999). Although the location of earthquakes and the position of volcanic arcs are routinely used to define the geometry of subducting slabs (Coney and Reynolds, 1977; Cahill and Isacks, 1992; Hayes et al., 2012), the distribution of intermediate-depth earthquakes in South America is spatially heterogeneous with apparent gaps along the trench (Fig. 1a, 1b), and the principal stress directions also deviate significantly from a simple configuration of flat slab (Anderson et al., 2007; Fig. 2). Consequently, the exact geometry of these flat slabs remains debated (Hayes et al., 2012; Anderson et al., 2007; Antonijevic et al., 2015) (Fig. 2). Furthermore, the two flat slabs in Peru and Central Chile do not show clear inland migration of arc volcanism (Antonijevic et al., 2015; Rosenbaum et al., 2005; Supplementary Figs. S1 and S2), suggesting that the flattening process of the slabs may be more complex than a mere reduction of local slab dip angle as traditionally assumed (e.g., Coney and Reynolds, 1977).

Second, recent seismic tomography has imaged fast shear-wave velocity (V_s) anomalies at ~70–100 km depth underlain by slow V_s anomalies in both the Peruvian (Antonijevic et al., 2015; Scire et al., 2016; Fig. 3) and Central Chilean flat-slab regions (Wagner et al., 2005; Young, 2014; Porter et al., 2012; Pesicek et al., 2012; Marot et al., 2014). Apparently, the nature of these seismic anomalies has important implications on the property of the overriding plate, the subducting slab, as well as the ambient mantle. Various explanations were proposed to interpret these seismic structures, including petrological anomalies due to dehydration reactions (Wagner et al., 2005), dry versus wet continental lithosphere (Marot et al., 2014), hydrated flat slab overlain by depleted mantle lithosphere (Porter et al., 2012; Wagner et al., 2006), or the flat slab sitting on a warm asthenosphere (Antonijevic et al., 2015; Pesicek et al., 2012; Calkins et al., 2008). As a result, the origin of these seismic anomalies remains uncertain.

Third, both the Peruvian and Central Chilean flat slabs are associated with magmatic formation of adakites (Gutscher et al., 2000; Figs. S1 and S2). On the one hand, since the chemical composition of adakite is similar to that of Archaean tonalite–trondhjemite–granodiorite (TTG), it has been proposed as a potential analogue

* Corresponding author.
E-mail address: jhu16@illinois.edu (J. Hu).

http://dx.doi.org/10.1016/j.epsl.2016.06.019
0012-821X/

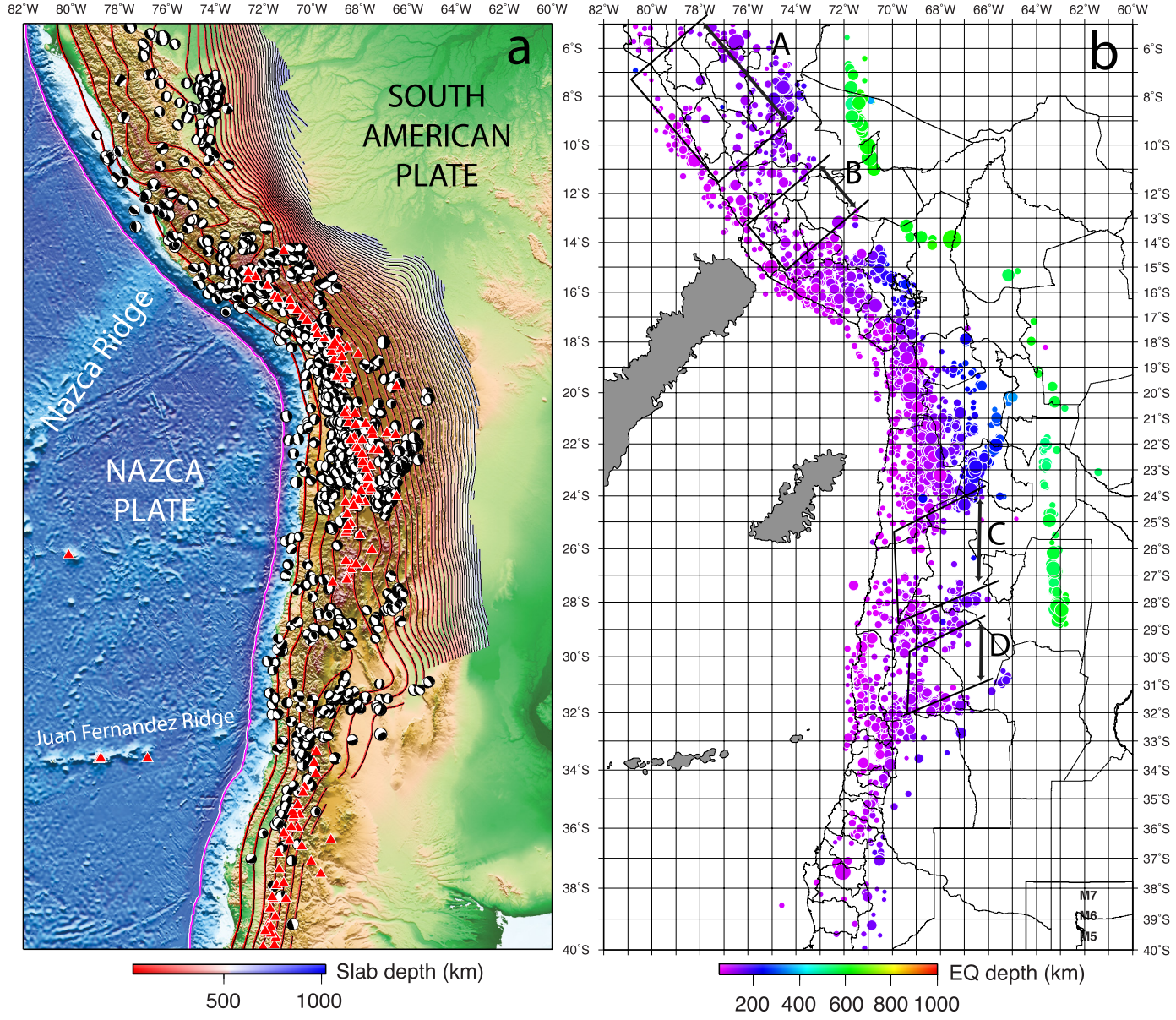

Fig. 1. Geological and geophysical settings of South American subduction zone. a) Topography of the western South America overlain by depth contours of the interpolated Benioff zones (Hayes et al., 2012), modern volcano locations based on www.ngdc.noaa.gov/hazard as well as CMT solutions from the IRIS database (ds.iris.edu/spud/momenttensor). b) Seismicity distribution with depth (>70 km) from the IRIS seismic catalog. Seismically quite regions are highlighted with brackets labeled with A, B, C, and D. We propose A, B and D may be caused by the subduction of Inca Plateau, Nazca Ridge and Juan Fernandez Ridge, respectively, while C is likely due to lithospheric delamination (Mulcahy et al., 2014). We used IRIS EMC (Trabant et al., 2012) to prepare the data in this figure. (For interpretation of the colors in this figure, the reader is referred to the web version of this article.)

for ancient continental growth (Drummond et al., 1996; Martin et al., 2005). On the other hand, the existence of adakites represents unusual (i.e., hot) thermal states of subduction zones, and thus may have important implications on subduction dynamics. Initially, the formation of adakites was attributed to the melting of young slabs (Drummond and Defant, 1990). However, this hypothesis was challenged with the discovery of adakitic suites over old subducting slabs (>25 Ma) (Macpherson et al., 2006). Consequently, many other models were proposed, for instance, melting of the subduction-eroded fore-arc crust (Kay and Mpodozis, 2002; Goss et al., 2013), flux-induced mantle melting that fractionates in the garnet-stable lower continental crust (Macpherson et al., 2006; Hidalgo and Rooney, 2014), melting of the thick arc crust (Petford and Atherton, 1996; Wang et al., 2005), as well as slab melting under various conditions (Sajona et al., 1993; Gutscher et al., 2000). Overall, the origin of adakites also remains controversial.

Here, we try to address these questions related to the Peruvian and Central Chilean subduction by investigating the temporal and spatial evolution of the South American flat-slabs. We performed a numerical simulation of the South American subduction history since 100 Ma, using geodynamic models with data assimilation (Hu et al., 2016). On the one hand, our model incorporates all major tectonic elements of past subduction including the plate motion history, seafloor ages, and a deformable Andean trench. On the other hand, we further consider the effects of tectonic features that are potentially related to flat-slab subduction, such as buoyant oceanic crusts, an over-thickened oceanic plateau (Inca Plateau) and two aseismic ridges (Nazca Ridge and Juan Fernandez Ridge) (Gutscher et al., 1999), and thick continental cratons (Fig. S3). Other model parameters that are more uncertain such as the viscosity structure of the background mantle and the downgoing slab are constrained by predicting the present-day slab ge-

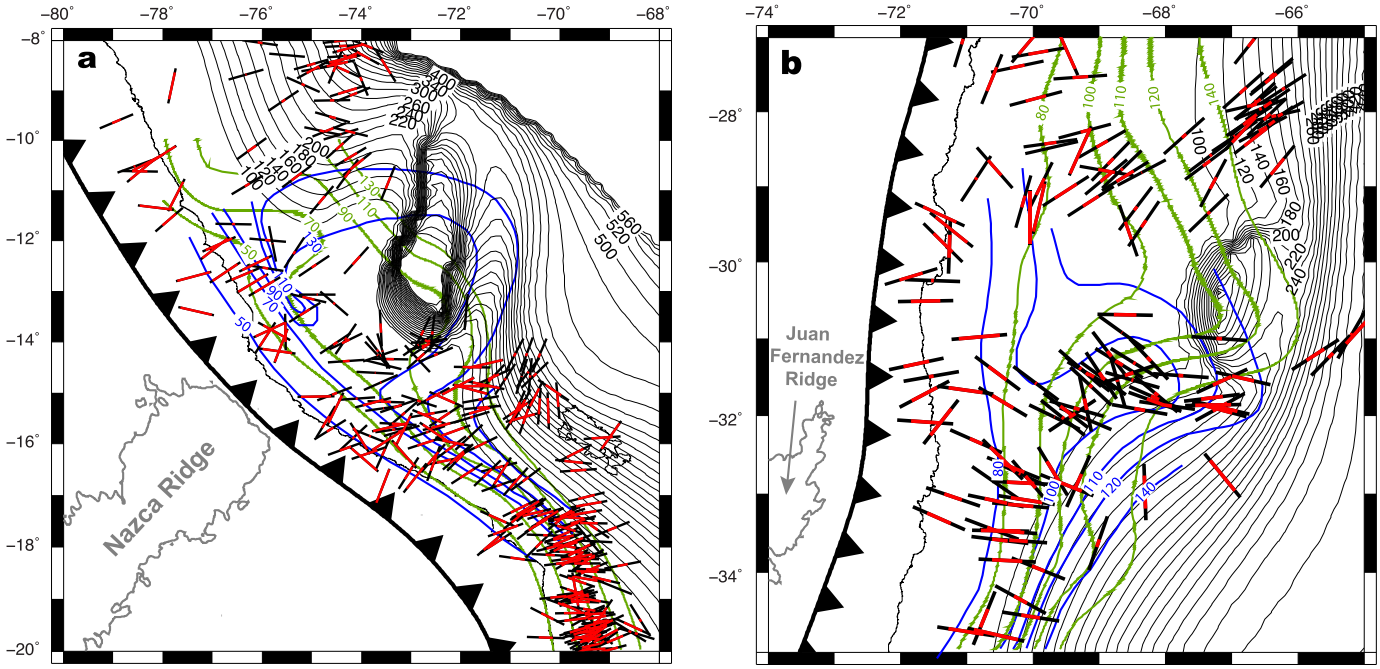

Fig. 2. Different proposed flat-slab geometries in Peru (a) and Central Chile (b) overlain by the earthquake T-axes of CMT solutions from the IRIS database (ds.iris.edu/spud/momenttensor). Green lines represent Benioff zone contours of slab 1.0. Blue lines are contours of two alternative models (Antonijevic et al., 2015 in (a); Anderson et al., 2007 in (b). Thin black lines are slab contours predicted from this study. Thick black bars with identical length indicate the azimuths of the T-axes, and the overlying red bars with variable lengths represent the horizontal components of the T-axes normalized by the total length of the vector. Therefore, a shorter red bar represents a stronger vertical component of T-axis, compared to a longer one. The observation that vertical component-dominated T-axes are mostly surrounding the slab tears outlines a chimney-configuration of the tearing slab, consistent with our model prediction. (For interpretation of the references to color in this figure legend, the reader is referred to the web version of this article.)

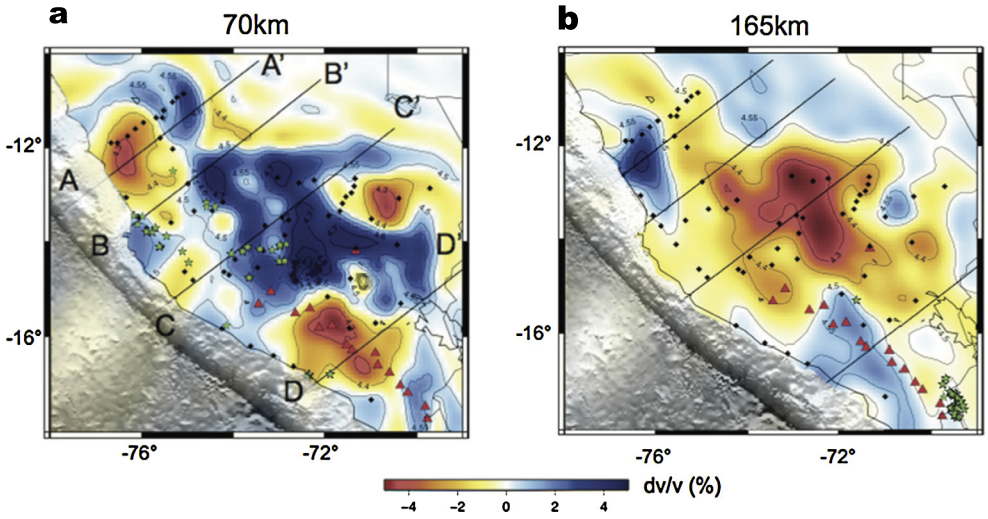

Fig. 3. Surface–wave tomography models at depth 70 km (a) and 165 km (b) showing the fast and slow V_s anomalies beneath the Peruvian flat slabs (from Antonijevic et al., 2015). (For interpretation of the colors in this figure, the reader is referred to the web version of this article.)

ometry (Hu et al., 2016) outlined with intra-slab seismicity distribution (Hayes et al., 2012) and seismic tomography images (Scire et al., 2015). Finally, we evaluate the abnormal seismological and magmatic observations using this constrained model of flat-slab subduction.

2. Methods

We use the finite element code CitcomS (Tan et al., 2006; Zhong et al., 2008) to solve thermal–chemical convection governed by the conservation of mass, momentum and energy. We assume that an incompressible mantle that has a variable viscosity and satisfies the Boussinesq approximation.

$$\nabla \cdot \vec{u} = 0 \tag{1}$$

$$-\nabla P + \nabla \cdot \left[\eta\left(\nabla\vec{u} + \nabla^T\vec{u}\right)\right] + (\rho_m \alpha \Delta T + \Delta\rho_c)\vec{g} = 0 \tag{2}$$

$$\frac{\partial T}{\partial t} + \vec{u} \cdot \nabla T = \kappa \nabla^2 T \tag{3}$$

$$\frac{\partial C}{\partial t} + \vec{u} \cdot \nabla C = 0 \tag{4}$$

where $\vec{u}$ is velocity, P dynamic pressure, T temperature, ρ_m the density of the ambient mantle, $\Delta\rho_c$ and ΔT the compositional density and temperature anomaly, respectively, η dynamic viscosity, and C composition; α, κ and $\vec{g}$ are thermal expansion coef-

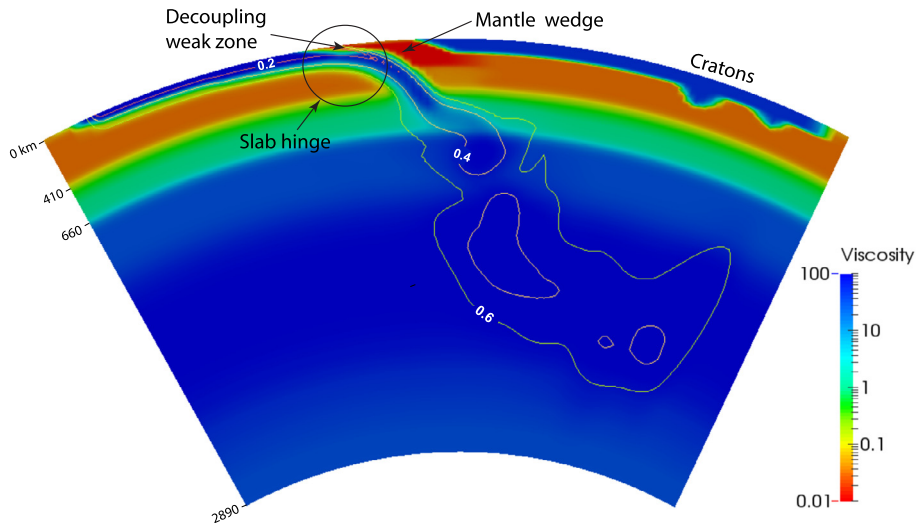

Fig. 4. Viscosity structure of an east–west cross-section at 20°S. Normalized viscosity is shown, with the reference viscosity being 10^{21} Pa s. The background viscosity follows a 4-layer profile from the lithosphere to the lower mantle. A uniform east-dipping narrow weak zone and a weak mantle wedge are on top of the slab in order to decouple the slab from the surface and to allow for asymmetric subduction. Because the maximum depth of the weak zone and the maximum viscosity cutoff within the slab hinge determine the slab strength, they are varied in Fig. 6 to test the robustness of the predicted slab tears. Over-plotted contours are isotherms with different values of the non-dimensional temperature. (For interpretation of the colors in this figure, the reader is referred to the web version of this article.)

ficient, thermal diffusivity and gravitational acceleration, respectively.

The model domain covers the region from 10°W to 100°W in longitude, 70°S to 20°N in latitude, and from the surface to 2890 km depth in radius, which is unevenly discretized by $257 \times 257 \times 65$ grids with the finest resolution of $27 \times 27 \times 8$ (km) in the upper central domain. Viscosity is both temperature- and composition-dependent, superimposed on a 4-layer background viscosity profile (Fig. 4): lithosphere (0–100 km), asthenosphere (100–300 km), transition zone (300–660 km), and lower mantle (660–2890 km). The background viscosity ranges from 3×10^{19} Pa s within the asthenosphere to 10^{23} Pa s within the lithosphere and at around 1500 km depth, while the transition zone viscosity is 10^{21} Pa s. The lower mantle viscosity increases from 660 km to about 1500 km depth, and then gradually decreases toward the core–mantle boundary. We also include a uniformly shallow-dipping weak plate interface (decoupling weak zone) along the subduction zone, a maximum viscosity cutoff within the slab hinge and a weak mantle wedge above the slab in our models to facilitate asymmetric subduction, similar to our earlier models (Liu and Stegman, 2011). This 3-D mantle viscosity structure is required to best match the present-day slab geometry as geophysical data reveal (Hu et al., 2016).

All models use free-slip sidewalls and core–mantle boundary, and imposed tangential velocities at the surface. The imposed surface plate motion is from a recent plate reconstruction by Müller et al. (2008). We use the seafloor age taken from the same plate reconstruction to define and update the thermal profile of oceanic lithosphere by assuming a modified error function based on the half-space cooling model (Hu et al., 2016). The continent is defined as a high viscosity sheet that has a thickness of 75 km. To simulate the dynamic suction force from cratons, we also parameterize thicker cratonic roots that extend to about 200 km depth. The geometry of the cratonic roots at 75 km depth follows that of Loewy et al. (2004), and their horizontal area shrinks as it goes from 75 km to 200 km depth. The temporally variable geometry of paleo-trenches is reconstructed by taking into account the shortening history of the central Andes (Arriagada et al., 2008). We use compositional tracers to represent the geometry and volume of oceanic crust, oceanic plateau and aseismic ridges. The buoyancy of these features is equivalent to an 8-km thick crust with a density of 2.9 g/cm^3, and 15-km thick oceanic plateau/aseismic ridges with the same density, respectively. More details about the geodynamic models could be found in Hu et al. (2016).

3. Results

3.1. Present-day slab geometry

Fig. 5 illustrates the predicted 3-D present-day slab geometry that best-fits the available observational constraints (Hu et al., 2016). In particular, this model successfully satisfies the overall shape of the Benioff zones along South America (Fig. 5a). Minor mismatches include a slightly shallower (steeper) predicted slab dip along the central Andes (northern Peru), compared to that outlined by seismicity (Hayes et al., 2012). The predicted slab geometry is also consistent with recent high-resolution tomography images (Scire et al., 2015). More importantly, the predicted along-trench variation of slab geometry closely matches the sharp slab curvature changes across the flat slab segments (Figs. 5a, S4 and S5).

Among the various proposed physical mechanisms for flat-slab formation including subduction of buoyancy features (Gutscher et al., 1999), hydrodynamic suction from a thick overriding plate (Manea et al., 2012), and fast overriding motion of continents (van Hunen et al., 2000), we find that the long-wavelength slab curvatures result from the viscous suction force from the overriding plate, and that the local flat slab geometry is mainly controlled by the subducting oceanic plateau and aseismic ridges (Hu et al., 2016). Therefore, it is the combined effects of these different mechanisms that lead to the observed present-day slab geometry along the entire South American trench.

An important result from these models is a major difference in the geometry of flat slabs from the traditional view: the central part of the flat slab tears apart with the two open limbs spanning a seemingly flat configuration (Figs. 5a, S4). In order to test the robustness of this model prediction, we perform three additional models by varying the viscosity structure of the slab hinge (Fig. 4), a key parameter controlling slab deformation (Fig. 6). These tests show that the slab tearing process does depend on slab-hinge viscosity and the degree of inter-plate decoupling. For example, the extent of slab tearing in Central Chile decreases (Fig. 6b–d) when

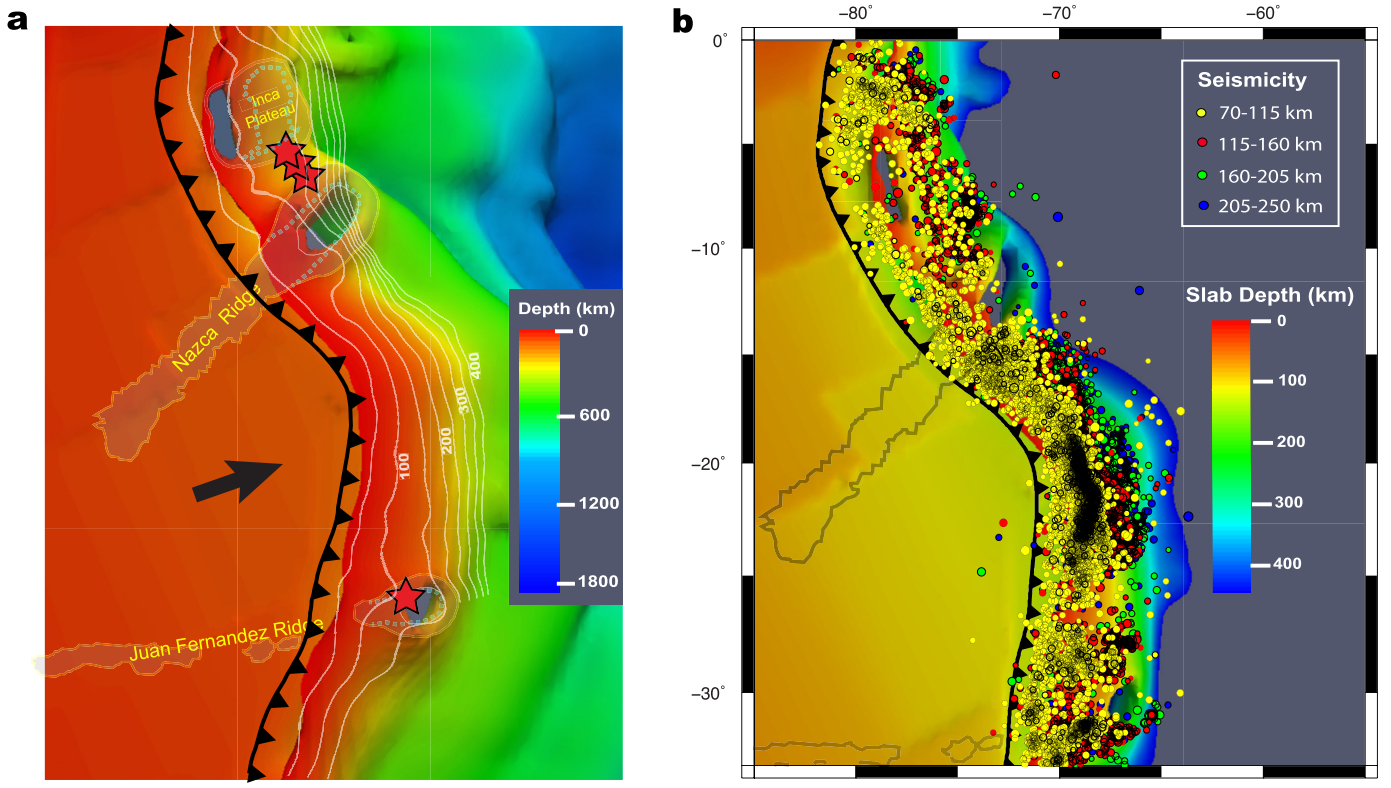

Fig. 5. 3-D geometry of the predicted present-day slab beneath South America and that of the Nazca Plate west of the trench (outlined using an isotherm of 300 °C cooler than the ambient mantle). a) 3D aerial view of the subducting Nazca Plate (temperature isosurface), with colors representing the depth of the slab's upper surface on the right side of the trench and depth of the plate's lower surface on the left side. The slab tears are illustrated with both the isosurface of temperature and the evolution of buoyancy features (translucent gray areas). Thin white lines are the interpolated Benioff zones from Hayes et al. (2012). Dashed lines within the subducting buoyancy features outline their original intact geometry. Red stars indicate the locations of adakitic eruptions. b) Map-view comparison of the slab geometry with the distribution of intermediate-depth seismicity ($M_b > 3.0$ from ISC seismic catalog). (For interpretation of the references to color in this figure legend, the reader is referred to the web version of this article.)

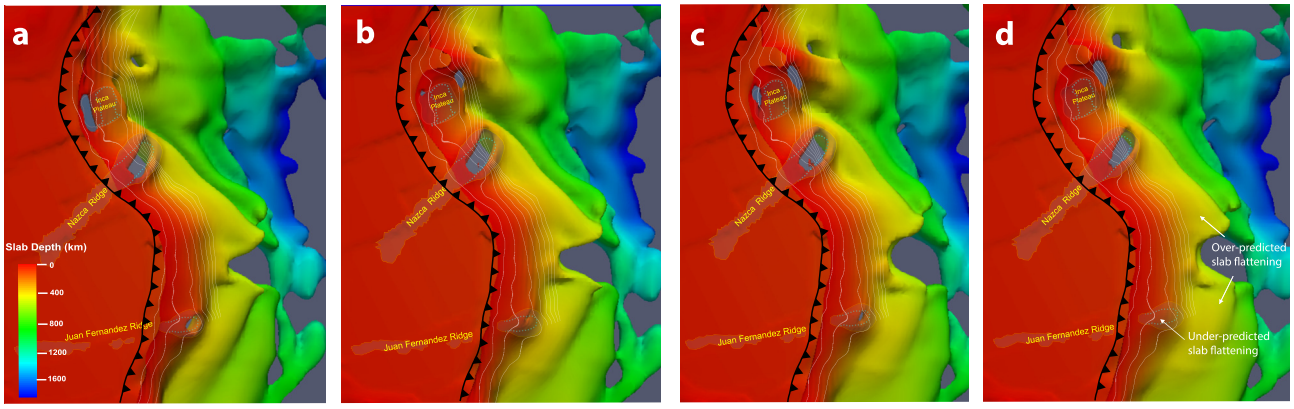

Fig. 6. The predicted present-day geometry of the subducting Nazca Plate (see Fig. 5 for a more detailed description) with different viscosity structures. a) The model with a decoupling weak zone extending from 0 to 120 km depth. The maximum viscosity at the slab hinge is 5×10^{22} Pa s. b) Same as (a), except that the decoupling weak zone terminates at 60 km depth. c) Same as (b), except that the maximum viscosity at the slab hinge is 7.5×10^{22} Pa s. d) Same as (b), except that the maximum slab hinge viscosity is 10^{23} Pa s. (For interpretation of the colors in this figure, the reader is referred to the web version of this article.)

the slab hinge becomes progressively stronger and the decoupling weak zone gets shallower, relative to those in the best-fit model (Fig. 6a). However, even in the case where the slab is the strongest (Fig. 6d), the Chilean flat slab still severely stretches and thins due to internal deformation caused by local buoyancy of the aseismic ridge. The fact that this model predicts a steeper Central Chilean slab but shallower slabs at greater depths than implied by the Benioff zones (Fig. 6d) suggests that this viscosity structure is inappropriate.

For the Peruvian flat slab, the tearing event is a robust model prediction as long as the subducting buoyancy feature is included in the simulation (Fig. 6a–d). We emphasize that the slab tear in visualization is defined for a given isotherm. This means a seemingly continuous slab outlined with a hotter isotherm (e.g., Fig. 6d) may appear torn when using a cooler isotherm. In general, these models suggest that a broken or severely stretched flat slab is required in order to best match the sharp slab dip variations associated with both the Peruvian and Central Chilean flat slabs (Figs. 5, 6). This internal slab deformation is confirmed by recent

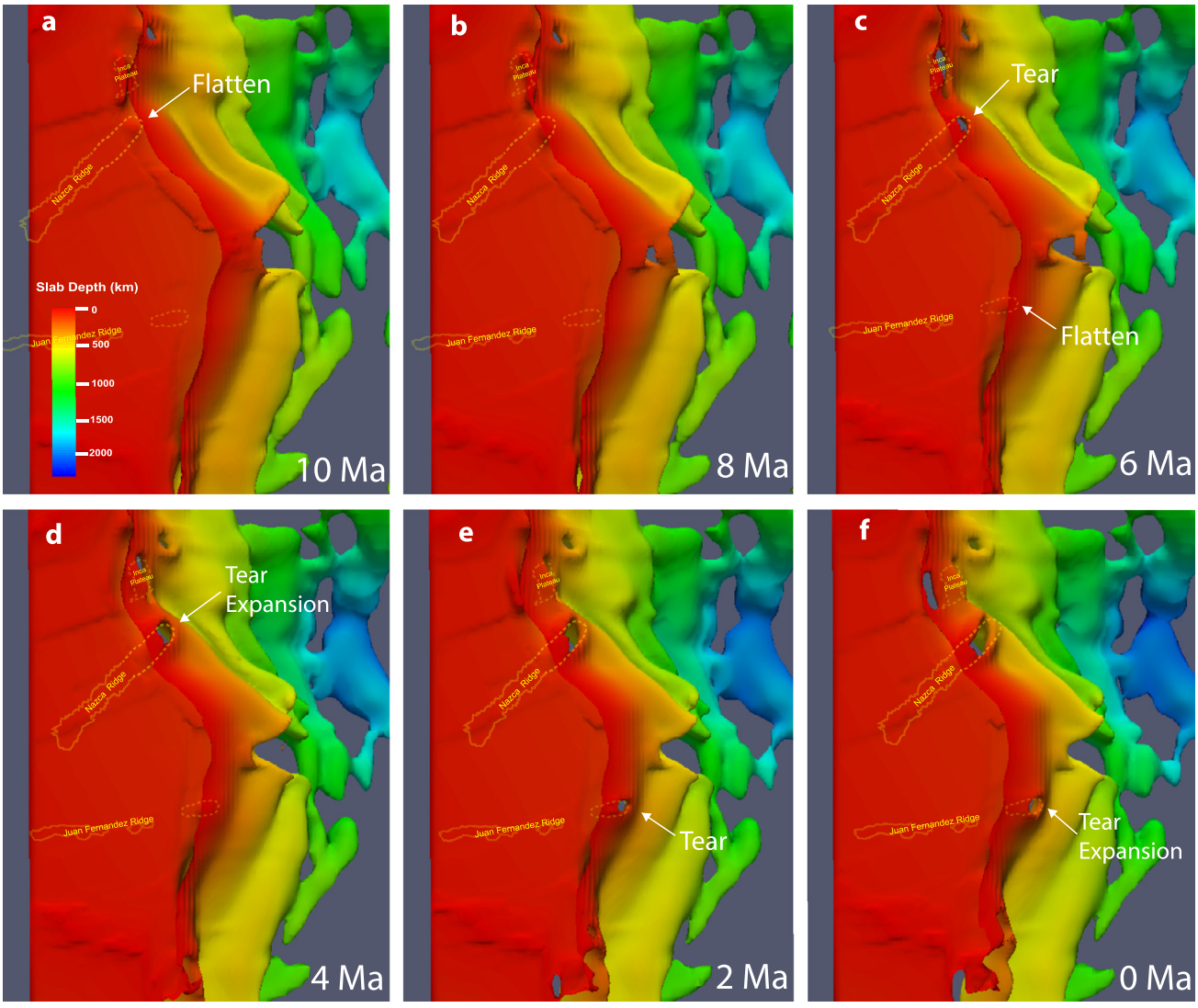

Fig. 7. 3-D view on the temporal evolution of the subducting Nazca Plate (outlined using an isotherm of 300 °C cooler than the ambient mantle) from 10 Ma to present day. The figure shows the evolution of initial slab flattening and deformation (a, b, d), and subsequent slab tearing and tear expansion (c–f) with time, for both the Peruvian and Central Chilean flat slabs. (For interpretation of the colors in this figure, the reader is referred to the web version of this article.)

seismic anisotropy measurements within the subducting Peruvian slab (Eakin et al., 2016). As we subsequently further demonstrate with more observational constraints, both these two flat slabs are very likely to be torn.

3.2. Formation of internal slab tears

In order to better understand the formation of these slab tears, we examine the temporal evolution of the flat-slab geometry during subduction of the buoyancy features (Figs. 7 and 8). We find that the initiation of the slab tear could be intuitively explained by the differential sinking rates between the subducting aseismic ridges and the surrounding slab portions: since the aseismic ridges are less dense than the surrounding slab (Gutscher et al., 1999), they tend to sink more slowly, which causes extensional strain to accumulate at the down-dip tips of these subducting ridges. Another way to think of this process is to consider the conservation of mass: since formation of the two prominent flat slabs requires an increase of local slab surface area relative to the steeply subducting parts (Fig. 6), the slab has to stretch internally. This can be seen from the subtle divergence of the horizontal velocity field across these growing slab tears and associated toroidal mantle flow around the open limbs of these slab tears (Fig. 8). Due to the localized distribution of buoyancy force within the aseismic ridges, this internal strain effectively stretches and thins the slab, eventually forming a gap. In contrast, the stress originated from hydrodynamic suction due to a thick overriding plate (Hu et al., 2016) is more distributed and temporally varying, and thus is less likely to cause the slab to tear (Taramón et al., 2015).

When subduction continues, the area of slab tear expands and the upper edge of the tear propagates toward the trench as the aseismic ridges subduct deeper (Fig. 7). The expansion of these slab tears is likely further related to the over-pressure of the sub-slab mantle (Liu and Stegman, 2011). The pressure beneath the slab is overall higher than that above because the slab's weight presses the mantle below but reduces the pressure above (Tovish et al., 1978). As a hole forms within the slab hinge, the high-pressure mantle beneath it pushes though the hole and moves upward; this local mantle upwelling warms up the surrounding slab and causes the slab to weaken further and the area of the slab tear to expand (vertical cross-sections in Fig. 8).

Furthermore, the temperature-dependence of slab strength suggests that a small extensional strain within the slab would quickly accumulate, because the positive feedback between temperature

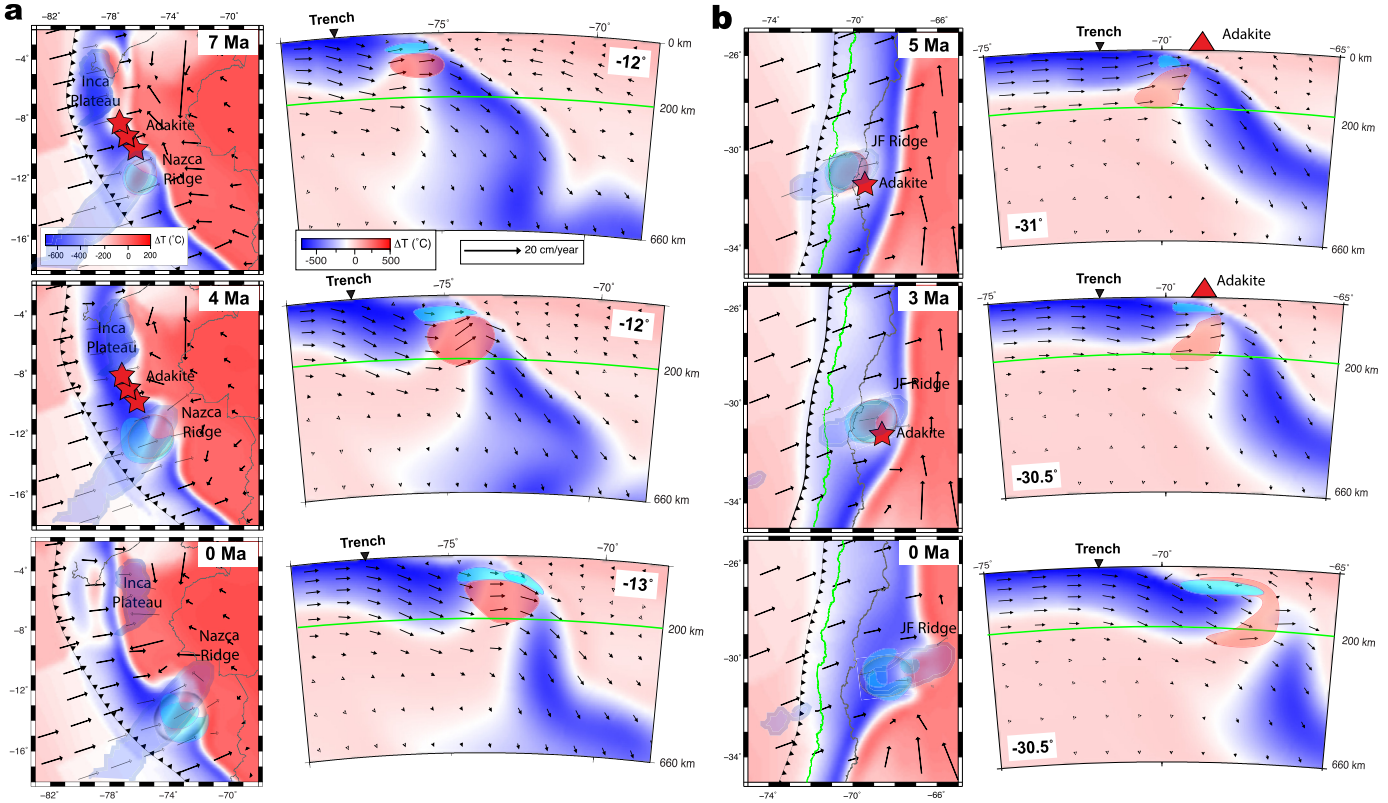

Fig. 8. 2-D view on the temporal evolution of the Peruvian (a) and central Chilean (b) slab tears. In each panel, both the map (left) and cross sectional (right) views are shown, corresponding to different times. All maps are at 100 km depth, and cross sections are E–W at the given latitude. The background color is for temperature (note the different color scales for the maps and cross sections) and arrows for velocity fields. The slab-tear induced upwelling likely generates partial melting (red transparent pattern), eclogitized crustal fragments at shallower depths (cyan transparent patterns) and adakitic eruptions (red stars in map views and triangles in cross sectional views). (For interpretation of the references to color in this figure legend, the reader is referred to the web version of this article.)

and viscosity facilitates strain localization. In addition, the strain-rate dependence of rheology, which is not included in our model, may further enhance this process (Arrial and Billen, 2013). In reality, possible existence of faults within the aseismic ridges during their emplacement into the subduction zone (Kopp et al., 2004) and a perturbed thermal structure due to the initial hot spot associated with the aseismic ridge (Yáñez et al., 2001) may also weaken the slab. Collectively, these factors should lead to stronger and faster local slab deformation compared to without. In our model, since the buoyancy features are the original source of stress for deformation to occur, the narrow aseismic ridges and oceanic plateaus ultimately become the location of slab detachment, which initiates at the down-dip end of these buoyancy features and propagates upwards as subduction continues (Figs. 7, 8).

According to our results, the formation of slab tears is associated with localized asthenosphere upwelling below these regions (Fig. 8). Dynamically, this upwelling is both passively driven by the outward extension of the flat slab (Figs. 6, 7) and actively driven by the excess sub-slab dynamic pressure as mentioned above (Liu and Stegman, 2011; Hu et al., 2016), which in the extreme case may form a large igneous province (Liu and Stegman, 2012). In Peru, strong localized upwelling occurred at 9 Ma along the eastern edge of the subducting Inca Plateau and at 4 Ma along the western edge of this Plateau as it further subducts (Fig. S6). Another phase of prominent upwelling started at 7 Ma along the down-going Nazca Ridge and sustained to the present (Fig. 8a). As subduction continues, these slab gaps and associated asthenosphere upwelling in Peru migrated southeastward (Fig. 8a). In Central Chile, a similar yet weaker upwelling started around 5 Ma when the slab tear initiated, and subsequently waned toward the present-day (Fig. 8b).

Formation of these slab tears explains several otherwise counter-intuitive observations. Since a slab tear releases sub-slab dynamic pressure (Stegman et al., 2006; Liu and Stegman, 2011) that initially facilitates slab flattening (Fig. 8), the mechanically detached frontal part of the slab would sink more easily than the intact rear part. Therefore, the larger slab gap inside the down-going Nazca Ridge than that in the Juan Fernandez Ridge explains why the former that has a greater buoyancy generates a shorter (~400 km) flat slab than that due to a less buoyant ridge in central Chile where the flat slab is ~700 km long (Figs. 5, S4; Hayes et al., 2012). Furthermore, the observation that the Inca Plateau that is shorter in the trench-normal direction than the aseismic ridges only partially tears along its edges (Fig. 5a), suggests that an oceanic plateau could likely translate a more intact flat slab far inland. This is consistent with the observation that a landward migration of volcanic arcs occurred over a large subducting oceanic plateau, best illustrated as the Late Cretaceous subduction of the Shatsky conjugate beneath western United States (Henderson et al., 1984; Liu et al., 2010). In contrast, a landward arc migration is largely absent during the Peruvian and Chilean slab flattening where aseismic ridges subduct (Rosenbaum et al., 2005) (Figs. S1 and S2). More implications of the slab tearing process are discussed in the next section.

3.3. *Abnormal seismological and volcanic observations controlled by tearing flat slabs*

Both the tearing flat-slab geometry and the associated asthenosphere upwelling provide new perspectives to better understand the abnormal seismological and volcanic observations along the South American subduction zone.

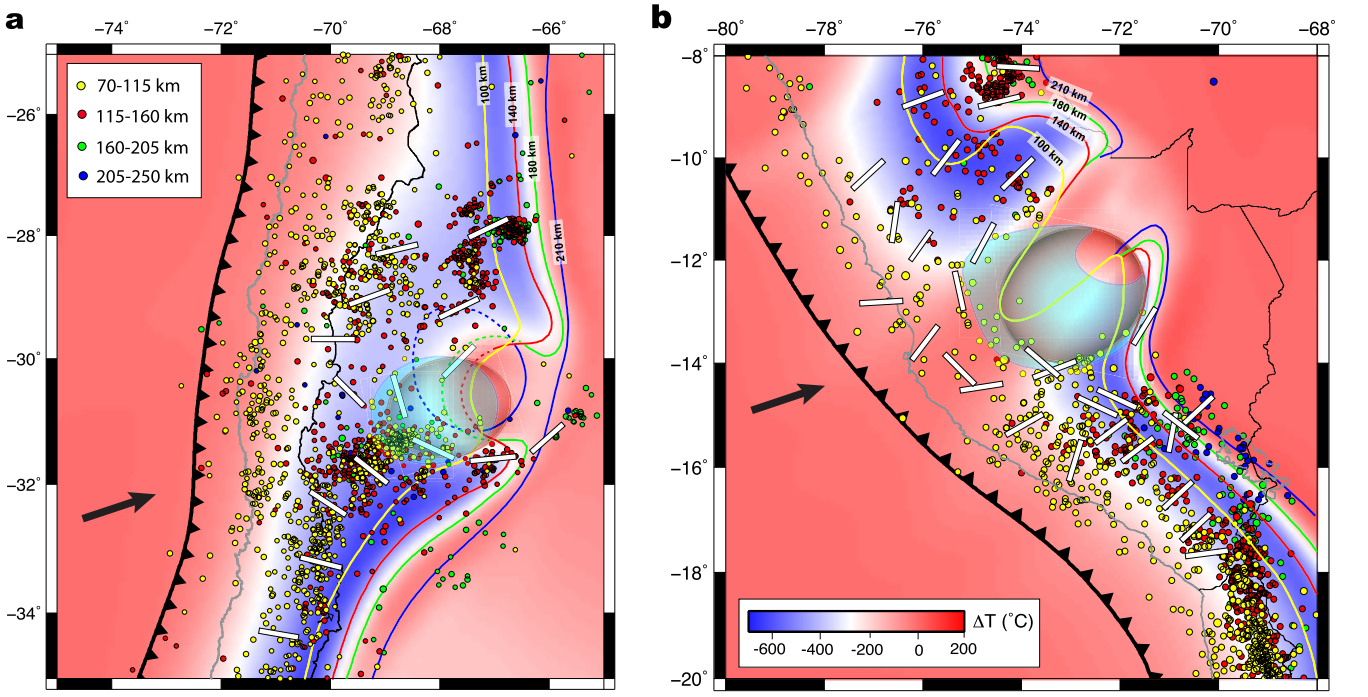

Fig. 9. Model comparison with seismic properties. a) Comparison of slab geometry (outlined using an isotherm of 200 °C cooler than the ambient mantle) at different depths (using different color lines) with seismicity ($M_b > 4.0$ from ISC seismic catalog, larger than the M_b threshold of 3.0 in Fig. 5b in order to show the background slab geometry). Overplotted are earthquake T-axis orientation (horizontal component; white bars) and the position of a vertical pair of slow (red sphere) and fast (cyan disk) V_s anomalies. b) Same as (a), but for the tearing Peruvian flat slab region. (For interpretation of the references to color in this figure legend, the reader is referred to the web version of this article.)

3.3.1. The distribution of intermediate-depth earthquakes

Our new flat-slab configuration naturally explains the enigmatic spatial variation of intermediate-depth (>70 km) seismicity along the South American trench (Brudzinski and Chen, 2005). At a glance, the map view (Fig. 5b) reveals a strong correlation between the three slab holes and a scarcity or lack of seismicity over these regions. All proposed models for the generation of intermediate-depth earthquakes require the presence of an oceanic lithosphere (Houston, 2007). Therefore, the predicted slab gaps explain the lack of seismicity in these regions, which are otherwise counter-intuitive since flat slabs likely concentrate large stresses and should, therefore, produce more earthquakes than the surrounding regions (Anderson et al., 2007). The other two regions in South America where reduced seismicity is observed are the equator and ~27°S (Fig. 5b), with the former corresponding to the subducting Carnegie Ridge (Fig. S7) that is not simulated in our model and the latter attributed to possible lithospheric delamination (Mulcahy et al., 2014).

To better understand the spatial correlation between earthquakes and slab configuration, we compare the detailed 3-D distribution of seismicity with the predicted slab geometry at four different depth ranges (Fig. 9). For each range, we plot earthquake epicenters with M_b magnitude >4.0, and compare their locations with the geometry of the slab at a similar depth. We note that earthquake location errors for these regions are about 10–30 km (Anderson et al., 2007; Dougherty and Clayton, 2015), which is minor compared to the overall slab dimension considered here. Fig. 9 reveals that almost all earthquakes fall into the slab interior at all depth ranges for both the Peruvian (Fig. 9b) and Chilean (Fig. 9a) slab segments. This provides another strong support to our model prediction, especially in Chile where high-resolution tomography is still lacking and the slab tear is more localized.

A closer examination of the modeled slab configuration suggests that the central Chilean slab gap with a west-downward tilting geometry between 30°S and 32°S is clearly delineated by the westward retreating seismicity distribution from 70 km to 200 km depths. The predicted reconnection of the slab below ~150 km depth on the eastern side also coincides with a chain of deep seismicity at a similar location (Fig. 9a). The predicted Peruvian slab gap (between 10°S and 14°S) goes largely vertically except near the trench where the slab reconnects at shallow depth (Fig. 9b). And this geometry is also delineated by the associated seismicity distribution, with the deeper side of the Peruvian slab gap aligned with some small-magnitude earthquakes (Fig. 5b).

3.3.2. The stress state of flat slabs

Our model results also better explain the unusual stress pattern of flat slabs in South America and, therefore, help to reconcile the existing debates on their geometry (Cahill and Isacks, 1992; Hayes et al., 2012; Anderson et al., 2007; Antonijevic et al., 2015). The analysis of earthquake focal mechanisms in Central Chile suggests a spatial pattern of slab stress (Anderson et al., 2007) (Fig. 9a) that is inconsistent with a wide flat slab traditionally defined by interpolating earthquake locations (Cahill and Isacks, 1992), and this stress pattern has been argued to imply a much narrower flat slab (Anderson et al., 2007) (Fig. 2b). Similarly in Peru, a recent tomography and focal mechanism analysis suggest a more localized flat slab (Antonijevic et al., 2015; Kumar et al., 2016), compared to that based on interpolated Benioff zones (Hayes et al., 2012) (Fig. 2a). From our model, the remarkable matches between the predicted tearing flat slabs and earthquake locations suggest that the debated flat slab geometry may be reconciled by realizing the existence of these internal slab tears.

More specifically, we examine the pattern of earthquake focal mechanisms by first plotting the representative horizontal component of T-axis (i.e., extensional stress direction, white bars in Fig. 9) inferred from relocated earthquakes in Central Chile (Anderson et al., 2007) and Southern Peru (Kumar et al., 2016). We can see that while the stress field to the north and south of these flat slabs is generally consistent with down-dip extension that is gen-

erally perpendicular to the trench, an obvious change in the T-axis orientation occurs both at 29°S–32°S (Fig. 9a) and at 10°S–15°S (Fig. 9b); they both form a quasi-circular pattern that strongly resembles the outline of the two slab tears. This intuitively suggests that the abnormal stress pattern reflects the spatial distribution of slab deformation during the formation of these tears (Figs. 7, 8).

By further analyzing the 3-D orientation of the dilatational focal mechanisms around the two flat slabs using data from IRIS (ds.iris.edu/spud/momenttensor), we find that most of the T-axes close to the edges of our predicted slab tears have a dominant vertical component over the horizontal one (Figs. 2a, 2b), and that those farther away from the two slab tears demonstrate a stronger horizontal component. This observation strongly reinforces our proposition that these T-axes outline the chimney-shaped slab edge geometry around the tearing flat slabs in both Peru and Chile (Figs. 2, 5, 9). Indeed, these T-axis orientations could be best interpreted as a superposition of the local down-dip direction following the highly distorted slab geometry and slab-edge parallel extension due to the expanding tears, with the former representing the major component of slab stress. Therefore, we conclude that our predicted broken slab geometry reconciles contrasting earlier hypotheses on the slab geometry using different observational proxies (Fig. 2), and that new insights on intra-slab earthquake formation emerge from these geodynamic simulations.

3.3.3. Seismic velocity structures

The asthenosphere upwelling associated with the breaking flat slabs helps to explain unusual seismic velocity structures below these regions. Recent shear-wave tomography imaged a fast V_S anomaly at depth between ~70 km and ~100 km in Central Chile, underlain by a slow V_S anomaly with a similar size (Wagner et al., 2005; Porter et al., 2012; Marot et al., 2014; Calkins et al., 2008). Interestingly, a recent ambient noise tomography investigating the Peruvian flat slab (Antonijevic et al., 2015) discovered similar seismic structures and with an even larger size (Fig. 3). Although the p-wave property of these fast V_S anomalies are uncertain or somewhat inconsistent among different studies (Wagner et al., 2005; Marot et al., 2014; Pesicek et al., 2012), reduced p-wave velocities associated with the slow V_S anomalies seem to be confirmed, especially in Peru (Scire et al., 2016; Marot et al., 2014; Pesicek et al., 2012). According to our models, both the present-day geometry and position of asthenosphere upwelling are consistent with those of the observed slow seismic anomalies (Figs. 3, 8, 9). This strong correlation suggests that the slow seismic anomalies very likely represent the hot asthenospheric mantle with possible partial melts due to decompression melting.

In contrast, the nature of the fast V_S anomalies is more elusive. If these structures have low p-wave velocities as proposed by Wagner et al. (2005), the resultant low V_P/V_S ratio of ~1.70 may indicate a highly depleted, pyroxene and Mg rich continental lithosphere (Wagner et al., 2006; Porter et al., 2012). A remaining question for this interpretation is why these lithosphere segments that are clearly outside of the tectonic cratons strongly correlate with the underlying slow seismic anomalies and the slab tears. If the fast V_S anomalies have fast p-wave velocities, they may instead represent the fragmented oceanic crusts. Since the flat slab has been thinned and stretched significantly, some oceanic crust could be easily stripped off and entrained by the asthenosphere upwelling. Due to the appropriate temperature and pressure conditions, these crustal fragments would easily convert to eclogite (Aoki and Takahashi, 2004), which at this depth range is seismically faster than both the continental crust (Anderson and Bass, 1984) and ambient mantle lithosphere (Worthington et al., 2013). Although future work is needed to further distinguish the above two scenarios, they both suggest that these fast V_S anomalies are not part of the flat slabs. Consequently, both these interpretations explain the apparent lack of seismicity in these regions, since these fast anomalies are mechanically decoupled from the subducting oceanic slabs (Fig. 8).

3.3.4. The formation of adakites

The upwelling asthenosphere beneath the tearing flat slabs also provides an ideal condition for the slab, especially its crust, to melt, which could be responsible for the formation of adakitic magmatism. In Central and South America, adakites formed above the subducting Chile Rise, Cocos Ridge, Carnegie Ridge, Nazca Ridge and Juan Fernendez Ridge (Gutscher et al., 2000). Among these, subduction of active mid-ocean ridges, such as Chile Rise and Cocos Ridge, can naturally result in slab melting (Drummond and Defant, 1990). But this is unclear for the latter three Ridges that are far away from spreading centers. Our model, with the asthenosphere upwelling beneath a tearing slab, provides a natural explanation for the observed adakites at these sites where the internal extension of the flat slab causes local temperature increase, which, together with the upwelling asthenosphere, could easily melt the much-thinned slab and its basaltic crust (Fig. 8).

In observation, adakitic eruptions in central Chile took place around 6-3 Ma, along ~31°S (Gutscher et al., 2000), which correlates remarkably with the initial formation of the slab gap (Fig. 8b). In Peru, the adakitic eruptions occurred along a ~300 km N–S distance range during 10–4 Ma (Gutscher et al., 2000). This process could have resulted from the joint contribution of slab tearing due to subduction of the Inca Plateau and the Nazca Ridge, during which toroidal flows advecting the hot mantle around local slab edges converge at the location of the adakite formation (Fig. 8a). Toward the present day, the cessation of adakitic eruption is largely correlated with the waning asthenosphere upwelling after the initially accumulated sub-slab dynamic pressure was released and with the gradual cooling of the mantle wedge as the slab further flattens (Fig. 8). These dynamic processes seem also consistent with the ore deposition history over these flat-slab segments (Rosenbaum et al., 2005).

4. Discussion

Our subduction model provides new perspectives for multiple enigmatic observations associated with the South American flat slabs. Consequently, this requires us to reconsider several consequences of flat slab subduction.

First, the mechanism for intermediate-depth earthquakes in Peru and Central Chile is uncertain. Currently, dehydration embrittlement (Raleigh and Paterson, 1965; Kirby et al., 1996; Peacock and Wang, 1999; Houston, 2007) represents a popular hypothesis for the cause of these earthquakes. Accordingly, Porter et al. (2012) suggest that the intermediate-depth seismicity in Central Chile occurs in the subducting oceanic mantle (Gans et al., 2011), where dehydration reaction of antigorite takes place (Kirby et al., 1996). They further suggest that the reduced seismicity below the front of the flat slab where steep subduction resumes, results from the cessation of dehydration, as the increased bending and extension within the upper half of the slab thickness release all the water (Porter et al., 2012). However, this hypothesis is not entirely consistent with the facts that the seismicity is already significantly diminished or absent along the flat part before the slab resumes steep subduction, especially in Peru (Figs. 1b and 9b) and that a small number of earthquakes reappear at greater depth below the inland portions of the flat slabs that are seismically quite (Figs. 5b and 9).

In order to reconcile this paradox, Kumar et al. (2016) propose that the thick crust due to the emplacement of the Nazca Ridge diminishes the initial hydration of oceanic mantle lithosphere, which limits the amount of subsequent mantle dehydration as the ridge

subducts, resulting in the reduced seismicity within the inboard projection of the Ridge. However, this explanation needs to be further verified, since dehydration embrittlement is not a fully confirmed hypothesis for intermediate-depth earthquake formation (Houston, 2007), and it is also unclear how the aseismic ridge could reduce the amount of hydration within the oceanic plate. In comparison, the slab gaps revealed by our model could explain both the reduced seismicity (Figs. 5, 9) and the slab stress state (Figs. 2, 9) more naturally, without the need to further modify the dehydration hypothesis. In addition, the locally elevated temperature of the torn or severely stretched flat slabs, below which hot mantle upwelling occurs, may be also responsible for the reduced seismicity.

Second, the exact geometry of flat slabs, especially that in Central Chilean, has been debated. Early receiver functions (Gilbert et al., 2006; Heit et al., 2008) could not resolve the flat slab due to the limited data coverage. As more regional seismic arrays are deployed, tomography models with relatively high resolution emerged. However, the presence of strong fast V_s anomalies at shallow depth (Wagner et al., 2005; Porter et al., 2012; Antonijevic et al., 2015), which were interpreted as depleted mantle lithosphere (Wagner et al., 2005) and/or eclogite converted from fragmented oceanic crust (this study), has severely obscured the detection of the down-going slab. Our best-fit model shows that in Central Chile much of the flat slab remains intact and the slab tear mainly occurs where the slab resumes steep subduction at the tip of the Juan Fernandez ridge. A more recent receiver function analysis by Gans et al. (2011) confirmed the existence of this flat slab on the west, but they could not resolve the slab geometry further east. In fact, Gans et al. (2011) observed multiple offsets of oceanic Moho depth trenchward of our predicted slab gap along the Juan Fernandez ridge and implies severe deformation within the flat slab, consistent with our model (Fig. 8). Alternatively, the flat slab in Central Chile may be severely deformed and thinned, but has not been fully torn apart yet (Fig. 6d). This slab configuration, alternative to our best-fit model, is still potentially consistent with the stress pattern and the adakitic magmatism above a localized mantle upwelling. However, this model is likely inconsistent with the distribution of intermediate-depth earthquakes. Nevertheless, the existing uncertainty in the mechanisms of intermediate-depth earthquakes requires more observational work to verify the existence of the Central Chilean slab gap.

Future research also needs to address several new questions raised from this study. In Peru, our modeling results show that the slab tear is a robust feature and has a lager slab gap compared with the one in Central Chile (Figs. 5 and 6), but its southern and northern edges are still continuous. This is consistent with the receiver function analysis by Phillips and Clayton (2014) that reveals a continuous southern side of the flat slab. However, along the northern side, Scire et al. (2016) imaged a ridge-parallel slab tear through body wave tomography, although the seismic resolution of this feature is limited. Antonijevic et al. (2015), based on ambient noise tomography, imaged a ridge-normal slab tear (Fig. 3) much closer to the trench and further north than that implied by both Scire et al. (2016) and this study. We suggest that the slab tear imaged by Antonijevic et al. (2015) could be related to the subduction of the Inca Plateau, although the latter is slightly more to the north (Figs. 5 and 8).

These inconsistencies between the two tomography models (Antonijevic et al., 2015; Scire et al., 2016) and with our geodynamical predictions also propagate into different interpretations of the observed fast V_s anomaly: the tomography model in Peru (Antonijevic et al., 2015) interprets the associated fast anomaly as part of the flat slab, but a similar fast anomaly in Central Chile is interpreted as depleted mantle lithosphere (Wagner et al., 2006; Porter et al., 2012; Marot et al., 2014). However, the fact that the fast V_s anomaly in Peru does seem to have a low V_p velocity as revealed by a recent body-wave tomography (Young, 2014) questions the slab interpretation. In addition, a new slab gap is tomographically detected at 33°S to the southeast of the Central Chilean flat slab (Anderson et al., 2007; Burd et al., 2013; Pesicek et al., 2012). This slab gap might be due to other dynamic processes, such as a locally hot mantle eroding the slab, which are not simulated in our model. Overall, the existing discrepancies in both seismic imaging and geodynamic interpretation suggest additional work is needed to better constrain the nature of these abnormal mantle structures.

Another outstanding question is the formation mechanism of adakites in South America. Petford and Atherton (1996) attributed adakites in Peru to be derived from the newly underplated basaltic sources. Kay et al. (1994) and Kay and Abbruzzi (1996) argued for melting of the over-thickened continental crust followed by delamination as the source of adakites in the Argentine–Puna Plateau. Kay and Mpodozis (2002) and Goss et al. (2013) proposed that the chemical signature of adakite in Central Chile was generated through the melting of the fore-arc crust that was eroded and transported by the slab into the mantle wedge. On the contrary, Gutscher et al. (2000) proposed that warming up of the leading edge of the flat slab as it propagates into the hotter asthenosphere accounts for the formation of adakite both in Peru and Central Chile.

While these hypotheses are probably petrologically feasible, they all seem to have limitations. For example, Kay and Kay (2002) pointed out that the underplating rate of basaltic magma proposed by Petford and Atherton (1996) is too slow to account for crustal thickening that is required for adakitic magmatism. They also questioned the slab melting model of Gutscher et al. (2000) by querying the existence of the 1200 °C isotherm at 60 km depth much east of the trench that is required by their model. On the contrary, Gutscher et al. (2000) argued that the crustal melting model of Kay et al. (1994) could not explain the paradox that adakitic eruption in Peru and Central Chile ceased in Pliocene but the thick crust preserves to the present. These arguments may not necessarily rule out the questioned hypotheses, due to the apparent complexity of geological processes. In stead, different hypotheses may account for different adakitic suites (Kay and Kay, 2002).

By reproducing the 4-D evolution of subduction, our model shows that the intense adakite production correlates well with the pulses of asthenosphere upwelling accompanying the slab tearing process. We propose that the asthenosphere upwelling may have significantly heated and partially melted the fragmented oceanic crust, which eventually leads to the formation of adakites. Therefore, our model is similar to Gutscher et al. (2000), but with a different geodynamic process to form slab melting. On the other hand, our model is not inconsistent with the "crustal melting" hypotheses. In these earlier models, a locally enhanced temperature is required in order to melt the crust to form adakites. Our model, by showing localized upwelling beneath a thinned or torn slab, provides the heat source for these models. In addition, the transient upwelling also gives a natural explanation for the short duration of adakitic magmatism which is not fully explained by the two "crustal melting" hypotheses (Kay et al., 1994; Kay and Abbruzzi, 1996; Kay and Mpodozis, 2002; Goss et al., 2013). To further narrow down on the exact mechanism, more research should focus on the detection of melt sources of these adakites.

5. Conclusion

In this paper, we present a new flat-slab configuration that reconciles multiple observations, including spatial discontinuities in intermediate-depth earthquake distribution, unusual slab stress

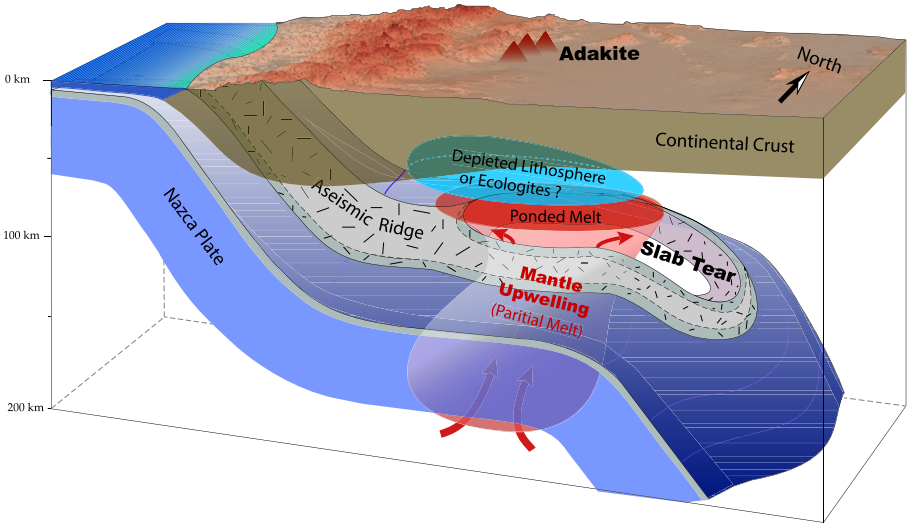

Fig. 10. Schematic representation of the broken flat slab during aseismic ridge subduction. In the overriding plate, only the crustal layer is shown. The vertical axis is exaggerated in scale.

patterns revealed by earthquake focal mechanisms, the elusive seismic anomalies around the flat slab regions, as well as the formation of adakites above the subducting aseismic ridges.

This new configuration of flat-slab subduction is illustrated in Fig. 10. The key feature is a down-dip oriented slab tear within the subducting aseismic ridge, where the two limbs of the broken slab span a geometry that is consistent with the traditional flat-slab geometry based on interpolated Benioff zones. Formation of the slab tear induces asthenosphere upwelling from beneath the slab, similar to processes occurring at a mid-ocean ridge (Key et al., 2013). The upwelling asthenosphere warms up and melts the severely stretched oceanic crust, leading to adakitic eruption and mineral enrichment at the surface during the initial stage of slab tearing. We propose that our discovered slab tearing events should represent a common consequence of flat-slab formation due to subduction of small to medium sized buoyancy features. The implied lithosphere buoyancy change and rheological variations due to the slab breaking process would likely affect the long-term dynamic evolution of the overriding continent.

Acknowledgements

We thank Xiaodong Song, Jay Bass and Craig Lundstrom for helpful discussions. The numerical models are performed using CitcomS (www.geodynamics.org) and GPlates (www.gplates.org). Figures are prepared using the GMT software package (https://www.soest.hawaii.edu/gmt/). This work is supported by NSF Grants ACI 1516586 and EAR-1554554.

Appendix A. Supplementary material

Supplementary material related to this article can be found online at http://dx.doi.org/10.1016/j.epsl.2016.06.019.

References

Anderson, D.L., Bass, J.D., 1984. Mineralogy and composition of the upper mantle. Geophys. Res. Lett. 11, 637–640.
Anderson, M., Alvarado, P., Zandt, G., Beck, S., 2007. Geometry and brittle deformation of the subducting Nazca Plate, Central Chile and Argentina. Geophys. J. Int. 171, 419–434.
Antonijevic, S.K., Wagner, L.S., Kumar, A., Beck, S.L., Long, M.D., Zandt, G., Tavera, H., Condori, C., 2015. The role of ridges in the formation and longevity of flat slabs. Nature 524, 212–215.
Aoki, I., Takahashi, E., 2004. Density of MORB eclogite in the upper mantle. Phys. Earth Planet. Inter. 143–144, 129–143.
Arriagada, C., Roperch, P., Mpodozis, C., Cobbold, P.R., 2008. Paleogene building of the Bolivian Orocline: tectonic restoration of the central Andes in 2-D map view. Tectonics 27 (6).
Arrial, P-A., Billen, M.I., 2013. Influence of geometry and eclogitization on oceanic plateau subduction. Earth Planet. Sci. Lett. 363, 34–43.
Brudzinski, M.R., Chen, W.-P., 2005. Earthquakes and strain in subhorizontal slabs. J. Geophys. Res. 110, B08303.
Burd, A.I., Booker, J.R., Mackie, R., Pomposiello, C., Favetto, A., 2013. Electrical conductivity of the Pampean shallow subduction region of Argentina near 33 S: evidence for a slab window. Geochem. Geophys. Geosyst. 14 (8), 3192–3209.
Cahill, T., Isacks, B.L., 1992. Seismicity and shape of the subducted Nazca Plate. J. Geophys. Res. 97, 17503–17529.
Calkins, J., Beck, S., Li, A., 2008. Lithospheric structure of the Pampean flat slab region of Chile and Argentina from analysis of Rayleigh wave propagation. PhD thesis. Univ. Arizona.
Coney, P.J., Reynolds, S.J., 1977. Cordilleran Benioff zones. Nature 270, 403–406.
Dougherty, S.L., Clayton, R.W., 2015. Seismic structure in southern Peru: evidence for a smooth contortion between flat and normal subduction of the Nazca Plate. Geophys. J. Int. 200 (1), 534–555.
Drummond, M.S., Defant, M.J., 1990. A model from trondhjemite–tonalite–dacite genesis and crustal growth via slab melting: Archaean to modern comparisons. J. Geophys. Res. 95, 21503–21521.
Drummond, M.S., Defant, M.J., Kepezhinskas, P.K., 1996. Petrogenesis of slab-derived trondhjemite–tonalite–dacite/adakite magmas. Spec. Pap., Geol. Soc. Am. 315, 205–215.
Eakin, C.M., Long, M.D., Scire, A., Beck, S.L., Wagner, L.S., Zandt, G., Tavera, H., 2016. Internal deformation of the subducted Nazca slab inferred from seismic anisotropy. Nat. Geosci 9 (1), 56–59.
Gans, C.R., Beck, S.L., Zandt, G., et al., 2011. Continental and oceanic crustal structure of the Pampean flat slab region, western Argentina, using receiver function analysis: new high-resolution results. Geophys. J. Int. 186 (1), 45–58.
Gilbert, H., Beck, S., Zandt, G., 2006. Lithospheric and upper mantle structure of central Chile and Argentina. Geophys. J. Int. 165 (1), 383–398.
Goss, A.R., Kay, S.M., Mpodozis, C., 2013. Andean adakite-like high-Mg andesites on the northern margin of the Chilean–Pampean flat-slab (27–28·5S) associated with frontal arc migration and fore-arc subduction erosion. J. Petrol. 54 (11), 2193–2234.
Gutscher, M.-A., Olivet, J.-L., Aslanian, D., Eissen, J.-P., Maury, R., 1999. The "lost Inca Plateau": cause of flat subduction beneath Peru? Earth Planet. Sci. Lett. 171, 335–341.
Gutscher, M-A., Maury, R., Eissen, J.P., et al., 2000. Can slab melting be caused by flat subduction? Geology 28 (6), 535–538.
Hayes, G.P., Wald, D.J., Johnson, R.L., 2012. Slab1.0: a three-dimensional model of global subduction zone geometries. J. Geophys. Res. 117, B01302.
Heit, B., Yuan, X., Bianchi, M., Sodoudi, F., Kind, R., 2008. Crustal thickness estimation beneath the southern central Andes at 30 S and 36 S from S wave receiver function analysis. Geophys. J. Int. 174 (1), 249–254.
Henderson, L.J., Gordon, R.G., Engebretson, D.C., 1984. Mesozoic aseismic ridges on the Farallon plate and southward migration of shallow subduction during the Laramide orogeny. Tectonics 3, 121–132.
Hidalgo, P.J., Rooney, T.O., 2014. Petrogenesis of a voluminous Quaternary adakitic volcano: the case of Baru volcano. Contrib. Mineral. Petrol. 168 (3), 1–19.
Houston, H., 2007. Deep earthquakes. In: Schubert, G. (Ed.), Treatise on Geophysics, vol. 4. Elsevier, pp. 321–350.

Hu, J., Liu, L., Hermosillo, A., Zhou, Q., 2016. Simulation of Late Cenozoic South American flat-slab subduction using geodynamic models with data assimilation. Earth Planet. Sci. Lett. 438, 1–13.

Kay, S.M., Coira, B., Viramonte, J., 1994. Young mafic back arc volcanic rocks as indicators of continental lithospheric delamination beneath the Argentine Puna plateau, central Andes. J. Geophys. Res., Solid Earth 99 (B12), 24323–24339.

Kay, S.M., Abbruzzi, J.M., 1996. Magmatic evidence for Neogene lithospheric evolution of the central Andean "flat-slab" between 30 S and 32 S. Tectonophysics 259 (1), 15–28.

Kay, R.W., Kay, S.M., 2002. Andean adakites: three ways to make them. Acta Petrol. Sin. 18 (3), 303–311.

Kay, S.M., Mpodozis, C., 2002. Magmatism as a probe to the Neogene shallowing of the Nazca plate beneath the modern Chilean flat-slab. J. South Am. Earth Sci. 15 (1), 39–57.

Key, K., Constable, S., Liu, L., Pommier, A., 2013. Electrical image of passive mantle upwelling beneath the northern East Pacific Rise. Nature 495, 499–502.

Kirby, S., Engdahl, R.E., Denlinger, R., 1996. Intermediate-depth intraslab earthquakes and arc volcanism as physical expressions of crustal and uppermost mantle metamorphism in subducting slabs. In: Subduction Top to Bottom, pp. 195–214.

Kopp, H., Flueh, E.R., Papenberg, C., et al., 2004. Seismic investigations of the O'Higgins Seamount Group and Juan Fernández Ridge: aseismic ridge emplacement and lithosphere hydration. Tectonics 23 (2).

Kumar, A., Wagner, L.S., Beck, L.S., et al., 2016. Seismicity and state of stress in the central and southern Peruvian flat slab. Earth Planet. Sci. Lett. 441, 71–80.

Liu, L., Gurnis, M., Seton, M., Saleeby, J., Muller, R.D., Jackson, J., 2010. The role of oceanic plateau subduction in the Laramide Orogeny. Nat. Geosci. 3, 353–357.

Liu, L., Stegman, Dave R., 2011. Segmentation of the Farallon slab. Earth Planet. Sci. Lett. 311, 1–10.

Liu, L., Stegman, D.R., 2012. Origin of Columbia River flood basalt controlled by propagating rupture of the Farallon slab. Nature 482, 386–389.

Loewy, S.L., Connelly, J.N., Dalziel, I.W., 2004. An orphaned basement block: the Arequipa–Antofalla Basement of the central Andean margin of South America. Geol. Soc. Am. Bull. 116 (1–2), 171–187.

Macpherson, C.G., Dreher, S.T., Thirlwall, M.F., 2006. Adakites without slab melting: high pressure differentiation of island arc magma, Mindanao, the Philippines. Earth Planet. Sci. Lett. 243 (3), 581–593.

Manea, V.C., Pérez-Gussinyé, M., Manea, M., 2012. Chilean flat slab subduction controlled by overriding plate thickness and trench rollback. Geology 40 (1), 35–38.

Marot, M., Monfret, T., Gerbault, M., Nolet, G., Ranalli, G., Pardo, M., 2014. Flat versus normal subduction zones: a comparison based on 3-D regional traveltime tomography and petrological modeling of central Chile and western Argentina (29°–35°S). Geophys. J. Int. 199, 1633–1654.

Martin, H., Smithies, R.H., Rapp, R., Moyen, J.F., Champion, D., 2005. An overview of adakite, tonalite–trondhjemite–granodiorite (TTG), and sanukitoid: relationships and some implications for crustal evolution. Lithos 79 (1), 1–24.

Mulcahy, P., Chen, C., Kay, S.M., Brown, L.D., Isacks, B.L., Sandvol, E., Heit, B., Yuan, X., Coira, B.L., 2014. Central Andean mantle and crustal seismicity beneath the Southern Puna plateau and the northern margin of the Chilean–Pampean flat slab. Tectonics 33. http://dx.doi.org/10.1002/2013TC003393.

Müller, R.D., Sdrolias, M., Gaina, C., Roest, W.R., 2008. Age, spreading rates, and spreading asymmetry of the world's ocean crust. Geochem. Geophys. Geosyst. 9 (4).

Peacock, S.M., Wang, K., 1999. Seismic consequences of warm versus cool subduction metamorphism: examples from southwest and northeast Japan. Science 286 (5441), 937–939.

Pesicek, J.D., Engdahl, E.R., Thurber, C.H., DeShon, H.R., Lange, D., 2012. Mantle subducting slab structure in the region of the 2010M8.8 Maule earthquake (30–40°S), Chile. Geophys. J. Int. http://dx.doi.org/10.1111/j.1365-246X.2012.05624.x.

Petford, N., Atherton, M., 1996. Na-rich partial melts from newly underplated basaltic crust: the Cordillera Blanca Batholith, Peru. J. Petrol. 37 (6), 1491–1521.

Phillips, K., Clayton, R.W., 2014. Structure of the subduction transition region from seismic array data in southern Peru. Geophys. J. Int. 196 (3), 1889–1905.

Porter, R., Gilbert, H., Zandt, G., et al., 2012. Shear wave velocities in the Pampean flat-slab region from Rayleigh wave tomography: implications for slab and upper mantle hydration. J. Geophys. Res., Solid Earth 117 (B11).

Raleigh, C.B., Paterson, M.S., 1965. Experimental deformation of serpentinite and its tectonic implications. J. Geophys. Res. 70, 3965–3985.

Rosenbaum, G., Giles, D., Saxon, M., Betts, P.G., Weinberg, R.F., Duboz, C., 2005. Subduction of the Nazca Ridge and the Inca Plateau: insights into the formation of ore deposits in Peru. Earth Planet. Sci. Lett. 239 (1), 18–32.

Sajona, F.G., Maury, R.C., Bellon, H., Cotten, J., Defant, M.J., Pubellier, M., 1993. Initiation of subduction and the generation of slab melts in western and eastern Mindanao, Philippines. Geology 21 (11), 1007–1010.

Scire, A., Biryol, C.B., Zandt, G., Beck, S., 2015. Imaging the Nazca slab and surrounding mantle to 700 km depth beneath the central Andes (18°S to 28°S). GSA Mem. 212.

Scire, Alissa, Zandt, George, Beck, Susan, Long, Maureen, Wagner, Lara, Minaya, Estela, Tavera, Hernando, 2016. Imaging the transition from flat to normal subduction: variations in the structure of the Nazca slab and upper mantle under southern Peru and northwestern Bolivia. Geophys. J. Int. 204 (1), 457–479.

Stegman, D.R., Freeman, J., Schellart, W.P., Moresi, L., May, D., 2006. Influence of trench width on subduction hinge retreat rates in 3-D models of slab rollback. Geochem. Geophys. Geosyst. 7 (3).

Tan, E., Choi, E., Thoutireddy, P., et al., 2006. GeoFramework: coupling multiple models of mantle convection within a computational framework. Geochem. Geophys. Geosyst. 7 (6).

Taramón, J.M., Rodríguez-González, J., Negredo, A.M., Billen, M.I., 2015. Influence of cratonic lithosphere on the formation and evolution of flat slabs: insights from 3-D time-dependent modeling. Geochem. Geophys. Geosyst. 16 (9), 2933–2948.

Tovish, A., Schubert, G., Luyendyk, B.P., 1978. Mantle flow pressure and the angle of subduction: non-Newtonian corner flows. J. Geophys. Res., Solid Earth 83 (B12), 5892–5898. http://dx.doi.org/10.1029/JB083iB12p05892.

Trabant, C., Hutko, A.R., Bahavar, M., Karstens, R., Ahern, T., Aster, R., 2012. Data products at the IRIS DMC: stepping Stones for research and other applications. Seismol. Res. Lett. 83 (5), 846–854. http://dx.doi.org/10.1785/0220120032.

van Hunen, J., van den Berg, A.P., Vlaar, N.J., 2000. A thermo-mechanical model of horizontal subduction below an overriding plate. Earth Planet. Sci. Lett. 182 (2), 157–169.

Wagner, L.S., Beck, S., Zandt, G., 2005. Upper mantle structure in the south central Chilean subduction zone (30° to 36°S). J. Geophys. Res. 110, B01308.

Wagner, L.S., Beck, S., Zandt, G., et al., 2006. Depleted lithosphere, cold, trapped asthenosphere, and frozen melt puddles above the flat slab in central Chile and Argentina. Earth Planet. Sci. Lett. 245 (1), 289–301.

Wang, Q., McDermott, F., Xu, J.F., Bellon, H., Zhu, Y.T., 2005. Cenozoic K-rich adakitic volcanic rocks in the Hohxil area, northern Tibet: lower-crustal melting in an intracontinental setting. Geology 33 (6), 465–468.

Worthington, J.R., Hacker, B.R., Zandt, G., 2013. Distinguishing eclogite from peridotite: EBSD-based calculations of seismic velocities. Geophys. J. Int. http://dx.doi.org/10.1093/gji/ggt004.

Yáñez, G.A., Ranero, C.R., Huene, R., et al., 2001. Magnetic anomaly interpretation across the southern central Andes (32–34 S): the role of the Juan Fernández Ridge in the late Tertiary evolution of the margin. J. Geophys. Res., Solid Earth, 6325–6345.

Young, B.E., 2014. Regional body-wave tomography of the Peruvian flat slab. Univ. of North Carolina at Chapel Hill.

Zhong, S., McNamara, A., Tan, E., et al., 2008. A benchmark study on mantle convection in a 3-D spherical shell using CitcomS. Geochem. Geophys. Geosyst. 9 (10).